Title

Temporal development of near-native functional properties and correlations with qMRI in self-assembling fibrocartilage treated with exogenous lysyl oxidase homolog 2

Authors

Hadidi, Pasha
Cissell, Derek D
Hu, Jerry C
et al.

Publication Date

2017-12-01

DOI

10.1016/j.actbio.2017.09.035

Peer reviewed

Acta Biomaterialia 64 (2017) 29–40

Contents lists available at ScienceDirect

Acta Biomaterialia

journal homepage: www.elsevier.com/locate/actabiomat

Full length article

Temporal development of near-native functional properties and correlations with qMRI in self-assembling fibrocartilage treated with exogenous lysyl oxidase homolog 2

Pasha Hadidi [a,1], Derek D. Cissell [a,1], Jerry C. Hu [b], Kyriacos A. Athanasiou [a,*]

[a] Department of Biomedical Engineering, University of California, Davis, One Shields Ave., Davis, CA 95616, USA
[b] Department of Biomedical Engineering, University of California, Irvine, 3120 Natural Sciences II, Irvine, CA 92697-2715, USA

ARTICLE INFO

Article history:
Received 24 June 2017
Received in revised form 22 September 2017
Accepted 25 September 2017
Available online 28 September 2017

Keywords:
Tissue engineering
Knee meniscus
Biomechanics
Self-assembling process
Cross-links
Quantitative MRI

ABSTRACT

Advances in cartilage tissue engineering have led to constructs with mechanical integrity and biochemical composition increasingly resembling that of native tissues. In particular, collagen cross-linking with lysyl oxidase has been used to significantly enhance the mechanical properties of engineered neotissues. In this study, development of collagen cross-links over time, and correlations with tensile properties, were examined in self-assembling neotissues. Additionally, quantitative MRI metrics were examined in relation to construct mechanical properties as well as pyridinoline cross-link content and other engineered tissue components. Scaffold-free meniscus fibrocartilage was cultured in the presence of exogenous lysyl oxidase, and assessed at multiple time points over 8 weeks starting from the first week of culture. Engineered constructs demonstrated a 9.9-fold increase in pyridinoline content, reaching 77% of native tissue values, after 8 weeks of culture. Additionally, engineered tissues reached 66% of the Young's modulus in the radial direction of native tissues. Further, collagen cross-links were found to correlate with tensile properties, contributing 67% of the tensile strength of engineered neocartilages. Finally, examination of quantitative MRI metrics revealed several correlations with mechanical and biochemical properties of engineered constructs. This study displays the importance of culture duration for collagen cross-link formation, and demonstrates the potential of quantitative MRI in investigating properties of engineered cartilages.

Statement of Significance

This is the first study to demonstrate near-native cross-link content in an engineered tissue, and the first study to quantify pyridinoline cross-link development over time in a self-assembling tissue. Additionally, this work shows the relative contributions of collagen and pyridinoline to the tensile properties of collagenous tissue for the first time. Furthermore, this is the first investigation to identify a relationship between qMRI metrics and the pyridinoline cross-link content of an engineered collagenous tissue.

1. Introduction

The knee meniscus is a critical fibrocartilage whose injury resulted in ~400,000 surgeries in the U.S. between 2005 and 2011 [1]. The knee meniscus bears and distributes loads for the underlying articular cartilage of the femoral condyle and tibial plateau, thereby preventing deterioration of these tissues within their highly demanding mechanical environment [2]. Loading of the meniscus occurs constantly throughout the day, and the tissue may be irreversibly damaged in a fraction of a second by a traumatic injury. The meniscus exhibits inability to heal due to its relatively avascular nature—only the periphery has a blood supply [3]. Without vasculature, regenerative growth factors and stem cells are unable to reach a site of injury, and, as a result, meniscus injury is commonly associated with long-term disability [4]. Moreover, the most common treatment to meniscus injury is partial meniscectomy, which may result in osteoarthritis [5]. These factors combine to make functional meniscus replacement a compelling clinical need.

* Corresponding author.
E-mail address: athanasiou@ucdavis.edu (K.A. Athanasiou).
[1] These authors contributed equally to this work.

https://doi.org/10.1016/j.actbio.2017.09.035
1742-7061/

The knee meniscus is a prime candidate for tissue engineering. In addition to the existing clinical need, the near-avascularity of fibrocartilage allows for the meniscus to be engineered in a relatively simple manner, largely without the need to reproduce a blood supply within the tissue. The outer one-third of the meniscus, or red-red zone, is vascularized, while the inner two-thirds, comprising the red-white and white-white zones, is largely avascular and thus more susceptible to lasting injury [3]. Therefore, it is appropriate to prioritize engineering the inner two-thirds of the knee meniscus. A surgeon may then attach an engineered implant to a native meniscal rim for integration. One approach to engineering tissue is to create a mechanically competent substitute for native tissue. Previous work from our laboratory has demonstrated the success of an approach known as the self-assembling process of cartilage, whereby scaffold-free tissues are able to reach native tissue values in terms of compressive properties [6–8]. The self-assembling process also allows for neotissue to be engineered in a variety of shapes and sizes [9]. This flexible design both replicates the wedged shape of the meniscus and allows for its maintenance in culture. The geometry of the meniscus is crucial for distributing load and providing stability within the knee joint after *in vivo* implantation [10]. Despite the advantages of the self-assembling process toward generating a viable meniscus replacement, there remains a need to improve tensile properties of scaffold-free tissues and more closely replicate the tensile strength and stiffness of the native meniscus.

An important relationship exists between the biochemical composition, microarchitecture, and viscoelastic mechanical properties of cartilage. Generally, the highly anionic glycosaminoglycan (GAG) molecules in cartilaginous extracellular matrix (ECM) confer compressive properties due to the ability of GAGs to bind and retain water. Collagen content, fiber diameter, and alignment generally confer tensile properties to cartilaginous tissues. The knee meniscus displays anisotropy due to its collagen microstructure, in which a high degree of collagen fiber alignment in the circumferential direction of the meniscus corresponds to a ~10-fold increase in tensile stiffness compared to the radial direction [3,11]. Furthermore, pyridinoline cross-links develop over time between collagen fibers and contribute to cartilage tensile properties [12,13]. Recent work has demonstrated the importance of pyridinoline collagen cross-links for improving tensile properties of engineered cartilage [13–15]. Further understanding the relationship between cartilage structure and function will improve efforts to replicate native tissue properties via tissue engineering.

Collagen cross-linking via pyridinoline represents an essential component in engineering fibrocartilage with proper mechanical integrity. Many tissue engineering efforts focus on collagen content or fiber orientation, yet collagen cross-linking comprises a relatively unexplored topic. Pyridinoline cross-links represent one type of molecular cross-linking which is associated with the development of collagen fibers natively. Although other types of cross-links exist in collagenous tissues, including pyrroles in mineralized tissues and arginoline in cartilage, pyridinoline cross-links are the most well-characterized and likely the most prevalent of these cross-links in cartilage [16,17]. The formation of pyridinoline cross-links is catalyzed by the lysyl oxidase (LOX) family of enzymes [18]. Prior work has demonstrated the transfection of LOX to enhance tensile properties of engineered vasculature [19]. Our laboratory has demonstrated the use of exogenous lysyl oxidase homolog 2 (LOXL2) to increase the tensile properties of articular cartilage and other musculoskeletal tissues [13]. However, the temporal characterization of long-term *in vitro* culture with LOXL2 is unexplored. This is particularly significant because the process of cross-link formation is believed to take weeks to months *in vivo* [17,20,21].

Clinicians commonly use conventional MRI to detect cartilage and fibrocartilage injuries in patients. Because conventional MRI is limited to the detection of cartilage tears or complete loss of cartilage, there has been interest in techniques that can detect early changes in cartilage that precede structural damage. Quantitative MRI (qMRI) measures inherent properties of tissues that influence how those tissues appear in a magnetic resonance image. Some qMRI techniques have been shown to be sensitive to changes in cartilage composition and/or stiffness that precede irreversible cartilage loss. Considerable research has been performed toward understanding the relationship between qMRI metrics and functional properties of native cartilage, including biochemical composition and compressive stiffness [22,23]. Further research has suggested that qMRI is a useful technique for non-destructive evaluation of tissue engineered cartilage *in vitro* [24–27]. For example, correlations were reported between the negative fixed charged density measured by qMRI and the compressive properties of tissue engineered cartilage [25]. To our knowledge, qMRI has never been applied to the assessment of self-assembling fibrocartilage. Furthermore, the effect of collagen cross-linking on MRI properties in self-assembling cartilaginous tissues has not been examined.

The objectives of this research were to examine the development of collagen cross-links over time, determine the contribution of collagen cross-links to mechanical properties, and to investigate the potential effect of cross-links on qMRI characteristics in engineered fibrocartilage. Toward these objectives, a two-factor, full factorial experimental design was employed. Self-assembling fibrocartilage constructs were cultured with or without LOXL2 treatment for varying culture durations. At the end of each prescribed culture duration, constructs were analyzed for gross morphology and samples tested for tensile properties, compressive properties, and qMRI. Samples of each construct were also prepared for quantitative biochemistry, HPLC, histology, and scanning electron microscopy (SEM). We hypothesized that (i) pyridinoline collagen cross-links would increase over time in culture, (ii) collagen and pyridinoline cross-links would both significantly contribute to self-assembling fibrocartilage tensile properties, and (iii) functional properties of self-assembling fibrocartilage would correlate with one or more qMRI metrics.

2. Materials and methods

2.1. Cell isolation

Primary cells were harvested from bovine hind limbs taken from skeletally immature calves, aged 4–8 weeks (Research 87). The femoral condyle and trochlea, as well as the white-white and white-red zones of the menisci, were minced into 1–3 mm^3 pieces and digested over several hours. The articular cartilage isolation consisted of an 18 h digestion with 0.2% collagenase type II (Worthington), while the meniscal tissue digestion consisted of 1 h of digestion with 0.25% pronase (Sigma-Aldrich) followed by an 18 h digestion with 0.2% collagenase type II [28]. Articular chondrocytes and meniscus cells were frozen in liquid nitrogen for storage after isolation. All native tissue controls were taken alongside the tissues used for cell isolation, and therefore were of the same age, maturity, and species.

2.2. Self-assembling tissue culture

After thawing from liquid nitrogen, primary articular chondrocytes and meniscus cells were seeded in non-adherent agarose wells in the shape of the knee meniscus [8]. Prior to seeding,

agarose wells were saturated for two days with a chondrogenic media formulation described previously [29]. Articular chondrocytes and meniscus cells were seeded in a 1:1 ratio at high density, totaling 10 million cells per construct [30], and cultured with chondrogenic media. A four-hour delay was allowed after initial seeding to prevent the self-assembling neotissue from being disturbed, after which cells were fed each day with 1 mL of chondrogenic media. After one week of culture, constructs were removed from their agarose wells and kept freely suspended in chondrogenic media for the remaining 7 weeks of culture. Lysyl oxidase-like 2 (LOXL2; Genway Biotech) administration occurred throughout weeks 2 and 3 of culture, along with the cofactors copper and free hydroxylysine, as described previously [15]. Constructs were grown for prescribed durations of either 1, 2, 3, 4, 5, 6, or 8 weeks and then assayed along with native tissue. For testing, samples were taken from various regions of the engineered constructs in a generally random fashion. Tensile samples were taken in the circumferential or radial directions, as illustrated in Fig. 1, from various regions of the constructs in a generally random fashion.

2.3. Histology and immunohistochemistry

Portions of constructs were embedded in HistoPrep (Fisher Scientific) at time points of interest and frozen at −20 °C. Samples and native tissue controls taken from the white-white zone were sectioned to a thickness of 14 μm and then stained. Picrosirius red and Safranin-O staining illustrated construct collagen and GAG content, respectively. Immunohistochemistry was performed using rabbit anti-bovine collagen I (Fitzgerald) and rabbit anti-bovine collagen II (Cedarlane) along with Vectastain ABC and DAB substrate kits (Vector Labs).

2.4. Tensile testing

Construct tensile properties were measured by a uniaxial, strain-to-failure test as previously described [30]. At week 1, due to the smaller size of each construct, a single dogbone-shaped sample in the circumferential direction was prepared and tested. At subsequent time points, two dogbone-shaped samples were prepared from each meniscus-shaped construct: one in the circumferential direction, and one in the radial direction. Tensile samples were photographed and their width (ranging from 0.17 mm to 0.56 mm) and thickness (ranging from 0.19 mm to 0.89 mm) were measured using ImageJ (ImageJ v. 1.48, National Institutes of Health). During each tensile test, paper tabs held each tensile sample affixed to a pre-determined gauge length (2.33 mm for dogbones in the circumferential direction and 1.33 mm for dogbones in the radial direction) using cyanoacrylate glue; metal grips then strained the paper tabs within a mechanical testing system (TestResources). Strain-to-failure tests were conducted at a constant strain rate of 1% of the gauge length per second and the load and displacement were recorded until failure occurred. The samples were observed throughout testing to ensure failure occurred in the narrowest portion of the dogbone. The relatively slow strain rate allowed time-dependent viscoelastic behavior to be ignored. A MATLAB (MATLAB R2013a, MathWorks, Inc.) program analyzed the stress-strain data to calculate the tensile Young's modulus and ultimate tensile stress (UTS) from the linear portion of the curve.

2.5. Compressive testing

Construct compressive properties were measured by stress-relaxation testing in unconfined compression using an Instron 5565 mechanical testing system (Instron Corporation) as previously described [31]. Briefly, a 2.5-mm diameter sample of each construct was prepared using a dermal biopsy punch. Each sample was photographed and its cross-sectional area measured using ImageJ. The sample was placed in a petri dish containing phosphate buffered saline and a non-porous platen approached each sample until a load of 0.04 N was observed, indicating contact with the sample; the position of the platen at this point indicated the sample thickness (ranging from 0.45 mm to 0.88 mm). Stress-relaxation testing was then performed; samples were preconditioned via 15 cycles of 5% strain, then subject to constant 10% strain for 360 s followed by 20% strain for 690 s. The strain rate for preconditioning and for each step strain was 10% per second. A MATLAB program analyzed the resulting stress-strain curves according to the standard linear solid model of viscoelasticity [31] to determine the samples' relaxation and instantaneous moduli and coefficients of viscosity.

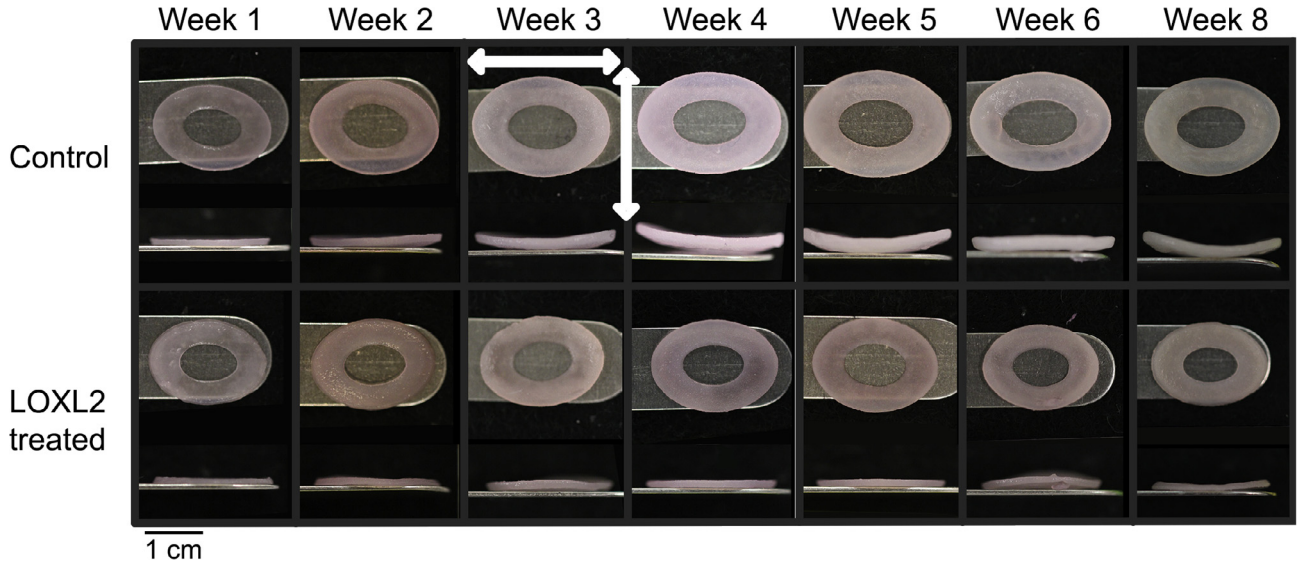

Fig. 1. Gross morphology of self-assembling, meniscus-shaped fibrocartilage. The white arrows on the week 3 control construct demonstrate the circumferential (horizontal arrow) and radial (vertical arrow) directions of the constructs, along which tensile testing occurred.

2.6. Quantitative biochemistry

A sample of each construct was used to determine its biochemical composition. Each biochemical sample was weighed and frozen at −20 °C at the end of its prescribed culture duration. A lyophilizer dehydrated frozen biochemical samples, and, following dehydration, each sample was re-weighed to determine the original water content. A papain solution digested dried samples, which were then analyzed for total collagen content via the hydroxyproline assay [32], for sulfated GAG content via the dimethylmethylene blue binding assay (Bicolor), and for DNA content via a fluorescent dye binding assay (Quant-iT PicoGreen, ThermoFisher Scientific).

2.7. High performance liquid chromatography

Portions of constructs were digested in 800 μL of 6 N HCl for 18 h at 100 °C to dissociate amino acids for high performance liquid chromatography (HPLC). Digested samples were dried in a vacuum and resuspended with 2.4 mM homoarginine and 10 μM pyridoxine. Following a 5-fold dilution with 0.5% heptafluorobutyric acid (HFBA), samples were injected into a Phenomenex column and eluted using a solvent profile, as previously described [33]. Pyridinoline standards (Quidel) were used to quantify cross-link content.

2.8. Quantitative magnetic resonance imaging

Portions from six control constructs and six LOXL2-treated constructs from half of the time points underwent quantitative magnetic resonance imaging (qMRI). An ~3 × 3 mm sample from each construct was placed in a custom, polyetherimide (Ultem™), 12-well plate. Chondrogenic media filled each well and care was taken to prevent and/or remove air bubbles. The well plate was centered in a 32 mm, ^{1}H-tuned, radiofrequency coil, which was in turn centered in a microgradient set within the bore of a 7T horizontal bore MRI system (Oxford Instruments Limited). After initial scout images were acquired, 1.5 mm thick slices were obtained through the center of each sample. The field of view for each image was 20 × 26 mm with an image matrix of 256 × 128 pixels and pixel size of 0.078 × 0.203 mm. Images were oriented such that three adjacent samples were imaged simultaneously and fine spatial resolution was achieved in the direction of the sample thickness. Appropriate pulse sequence specifications for quantification of T1 time, T2 time, and apparent diffusion coefficient (ADC) are given in Table 1. For T2 measurement, single-echo, spin echo images were acquired for each prescribed echo time to minimize error associated with B_1 field inhomogeneity and incomplete refocusing of multiple echoes in an echo train. All images were obtained using multi-slice acquisition with a single excitation per image (i.e., NEX = 1). Free-form regions of interest (ROI) were drawn around each sample and the signal intensity for each sample and pulse sequence measured using Paravision v. 4.0 image analysis software (Bruker Biospin Corporation). T1 times and ADC's were calculated using Paravision; T2 times were calculated using MATLAB.

Table 1
Quantitative MRI pulse sequence specifications.

	Fixed parameter(s)	Variable parameter
T1	TE = 20.8 ms	TR = 250, 500, 1000, 1600, 2400, 3600, 5400 ms
T2	TR = 5400 ms	TE = 11.65, 23.25, 46.5, 69.3, 93.0 ms
ADC	TR = 3000 ms; TE = 18.4 ms	b = 5, 130, 255, 505, 1005 s/mm^2

TE, echo time; TR, repetition time; b, diffusion weighting; ADC, apparent diffusion coefficient.

2.9. Scanning electron microscopy

Portions of constructs were suspended in 50 mM cacodylate buffer with 2.5% glutaraldehyde and 5% sucrose at 4 °C to prepare for SEM. After ethanol dehydration, a critical point dryer and gold sputter coater dehydrated and plated samples, respectively, prior to imaging using a Phillips XL30 TMP scanning electron microscope. Images were taken over different areas from multiple samples per group. The threshold function in ImageJ allowed for determination of ECM density in tissue samples. Representative images were divided into nine equal sub-regions, of which three were chosen randomly and used to quantify average fiber diameter.

2.10. Statistical analysis

All results are expressed as mean ± one standard deviation. For this study, n = 7 constructs per group. One-way ANOVA examined differences among groups with *post hoc* analysis by Tukey's honest significant difference method, as indicated using JMP Pro 12 statistical analysis software (SAS Institute). JMP also assessed pairwise correlations among properties. MATLAB analyzed residual terms to confirm normality, independence, constancy of variance, and to detect outliers. Response data were log-transformed and/or outliers were removed and ANOVA repeated, if necessary, to correct normality and constancy of variance. Statistical significance was defined by $p < 0.05$. Stepwise linear regression was used to screen for potential combinations of biochemical properties contributing to variation in qMRI properties. Statistical models were limited to a maximum of four factors, and the best models were selected based on minimum Bayesian information criterion and minimum corrected Aikake information criterion. The best three models were assessed by multiple linear regression. Selected multi-factor correlations were examined using multiple linear regression (MLR). Scaled coefficient estimates for each significant factor in the MLR model were calculated by fitting the response data to factors centered by mean and scaled by the range divided by two. For multi-factor correlations, the R^2-adjusted coefficient (R^2_{adj}) was calculated to correct for potential spurious increases in the correlation coefficient associated with multiple factors. Statistically significant correlations were defined as weak, moderate, or strong for R^2 values less than 0.3, between 0.3 and 0.5, or greater than 0.5, respectively.

3. Results

3.1. Gross morphology, histology, and immunohistochemistry

In general, the control group of constructs increased in diameter and thickness over time (Fig. 1). Constructs in the control group also tended to develop a slightly curved morphology that was first apparent after week 3 of culture and persisted in most constructs through later culture durations. In contrast, LOXL2-treated constructs were smaller in diameter and thickness at all time points after week 1 and tended to have a flatter morphology. Both control and LOXL2-treated constructs exhibited a wedge shape on cross-section that was thinner toward the inside of the ring and thicker at the outside of the ring. Construct gross morphology did not demonstrate any clear trends of heterogeneity.

Control and LOXL2 constructs significantly increased in length from 10.2 ± 0.1 mm at 7 days (both groups) to 11.9 ± 0.2 mm (control) and 11.0 ± 0.1 mm (LOXL2) at 21 days of culture. Control constructs continued to increase to a final length of 13.9 ± 0.4 mm at 56 days, whereas LOXL2 constructs did not significantly increase in length after 21 days and measured 11.1 ± 0.2 mm at 56 days. Control constructs were significantly longer than LOXL2 constructs

at all culture durations after 7 days. Similarly, control and LOXL2 constructs significantly increased in thickness from 0.52 ± 0.03 mm (control) and 0.48 ± 0.05 mm (LOXL2) at 7 days to 0.94 ± 0.11 mm (control) and 0.60 ± 0.06 mm (LOXL2) at 21 days of culture. Control constructs continued to increase to a final thickness of 1.29 ± 0.23 mm at 56 days, whereas LOXL2 constructs did not significantly increase in length after 21 days and measured 0.63 ± 0.06 mm at 56 days. Control constructs were significantly thicker than LOXL2 constructs at all culture durations after 7 days.

In terms of staining, all constructs stained positively for collagen, GAG, and collagen types I and II (Fig. 2). Furthermore, LOXL2-treated constructs stained more similarly to native white-white zone meniscus tissue than constructs from the control group. Picrosirius red staining for collagen showed slightly more intense staining in the LOXL2-treated constructs at weeks 4 and 8 of culture, while Safranin-O staining for GAG was more intense among control constructs. Constructs did not display obvious heterogeneity in histological staining.

3.2. Tensile properties

Tensile properties of control group constructs and LOXL2-treated constructs remained similar over time (Fig. 3), until the tensile properties of LOXL2-treated constructs eventually displayed a 3.3- to 3.7-fold increase over control group values after 8 weeks of culture. The tensile properties of the LOXL2-treated constructs increased throughout culture, and were significantly greater than the control group constructs by week 6 of culture. In contrast, the tensile properties of the control group decreased by week 8 of culture, with stiffness in the circumferential direction decreasing by 40% as compared to week 6.

LOXL2-treated constructs reached their largest values at week 8 of culture. After 8 weeks of culture, tensile stiffness as measured by Young's modulus reached 5.65 ± 0.14 MPa in the circumferential direction (9% of native tissue values) and 3.33 ± 1.43 MPa (65% of native tissue values) in the radial direction. Similarly, ultimate tensile strength reached 1.34 ± 0.22 MPa in the circumferential direction (5% of native tissue values) and 1.10 MPa ± 0.17 MPa (26% of native tissue values) in the radial direction. By comparison, at week 8 of culture, control constructs displayed a Young's modulus of 1.77 ± 0.49 MPa and a UTS of 0.38 ± 0.072 MPa in the circumferential direction. At the same time point, control constructs displayed a Young's modulus of 0.94 ± 0.29 MPa and a UTS of 0.30 ± 0.13 MPa in the radial direction.

3.3. Compressive properties

The instantaneous and relaxation moduli at 10% strain increased with increasing culture duration in both the control and LOXL2-treated groups (Fig. 4). It should be noted that compressive data were log-transformed and two outliers (one each from the 2- and 4-week control groups) were removed to correct constancy of variance and normality of the residual terms. After two weeks of culture, the compressive stiffness of control constructs was significantly greater than in LOXL2-treated constructs, and this difference increased throughout culture. After 8 weeks of culture, instantaneous and relaxation moduli were 351 ± 68 kPa and 199 ± 45 kPa, respectively, for control constructs and 137 ± 39 kPa and 48 ± 13 kPa, respectively for LOXL2 constructs (all values at 10% strain).

The coefficient of viscosity also increased throughout culture for the control groups from 0.55 ± 0.07 MPa·s to 4.4 ± 1.1 MPa·s. In contrast, the coefficient of viscosity remained unchanged throughout culture for LOXL2-treated constructs and was less than that of control constructs (0.61 ± 0.26 MPa·s at week 8). At 8 weeks of culture, LOXL2-treated constructs exhibited similar relaxation moduli to native meniscus while control constructs were much stiffer than native meniscus. At this time point, both control and LOXL2 constructs had lower instantaneous moduli than native meniscus, and control constructs exhibited instantaneous moduli that were closer to native values. The coefficient of viscosity for native meniscus was approximately half-way between the coefficients of viscosity for control and LOXL2 constructs.

3.4. Biochemistry and HPLC

Results of biochemical analysis are summarized in Fig. 5. GAG/DW increased from ~17% at week 1 in both control and LOXL2 constructs to 57.6 ± 5.3% in control constructs and 33.8 ± 4.6% in LOXL2 constructs at week 5. Both groups exhibited transient

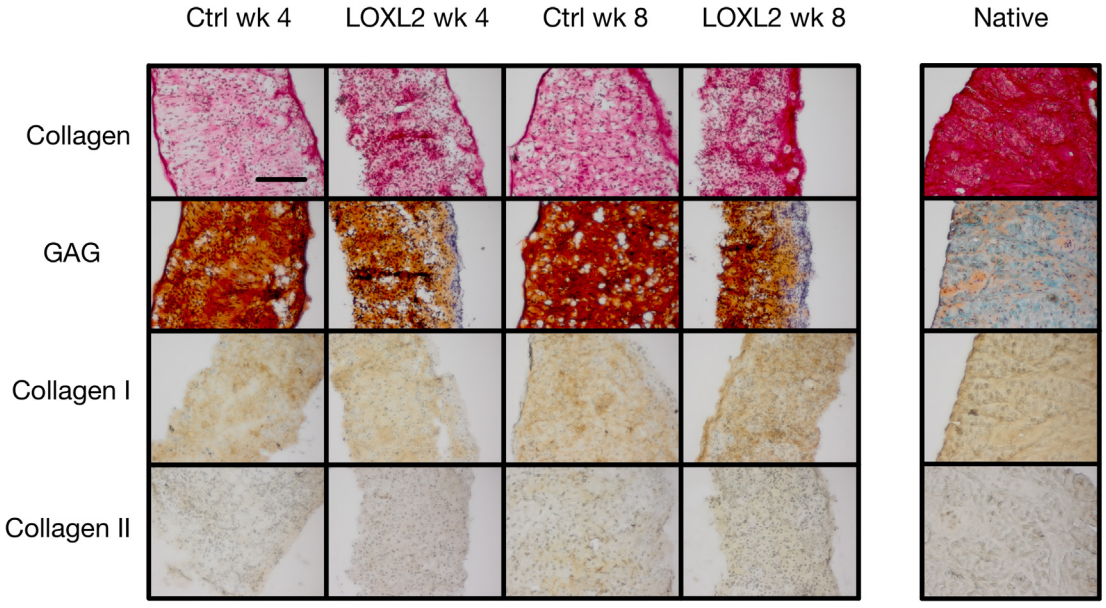

Fig. 2. Histology and immunohistochemistry of self-assembling, meniscus-shaped fibrocartilage. All samples are presented as slices through the thickness of the tissue, with the circumferential direction running from top to bottom of each photograph. Native controls taken from white-white zone, scale bar represents 200 μm.

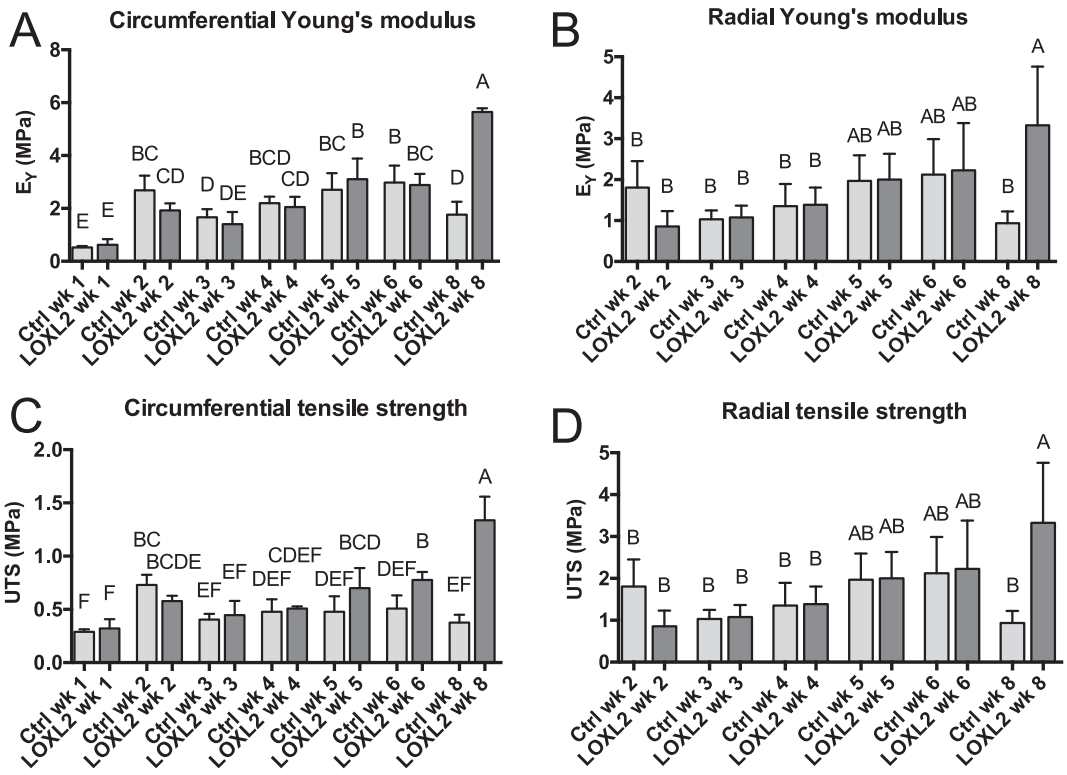

Fig. 3. Tensile properties of self-assembling, meniscus shaped fibrocartilage. Native tissue values: 65.7 ± 32 MPa (circumferential Young's modulus), 24.3 ± 14 MPa (circumferential UTS), 5.09 ± 2.9 MPa (radial Young's modulus), 4.23 ± 2.3 MPa (radial UTS). Groups lacking a letter in common are significantly different.

decreases in GAG/DW at the 6-week time point before rebounding to 64.1 ± 5.2% in the control group and 32.9 ± 5.8% in the LOXL2 group at the final time point. At every culture duration beyond week 2, control constructs contained significantly more GAG/DW than LOXL2 constructs at the same time point. Collagen/DW began at 5.3 ± 0.5% in both groups at week 1 and increased to a maximum of 13.7 ± 1.2% in the LOXL2 group at 8 weeks. Control constructs developed a maximum of 11.5 ± 1.9% collagen/DW at week 5 of culture, and then remained between 9.9 and 10.9% collagen/DW at subsequent time points with no significant differences among the control constructs from week 2 to week 8 of culture. DNA/DW decreased over time, starting from 16.3 ng DNA/μg tissue to 6.1 ng DNA/μg tissue in LOXL2 constructs and 2.9 ng DNA/μg tissue in the control constructs at week 8.

Cross-link content in LOXL2-treated constructs began increasing midway through culture, significantly exceeded control values, and eventually approached native tissue values. Cross-link content was consistently greater in LOXL2-treated constructs. A 5.4-fold increase in cross-link content over controls was seen in LOXL2-treated constructs at week 4, and this increase grew to a dramatic 9.9-fold change by week 8 of culture. Prior to week 4, no significant changes in cross-link content were detected between control and LOXL2-treated constructs. After 8 weeks of culture, cross-link content in LOXL2-treated constructs reached 907.46 ± 129.15 nmol/g (77% of native tissue values) as compared to 92.34 ± 25.56 nmol/g for control constructs.

3.5. Correlations between composition and mechanical properties

Strong correlations were observed between construct compressive properties and GAG content. As construct GAG content increased, relaxation modulus, instantaneous modulus, and coefficient of viscosity all increased (Fig. 6). Correlations were strongest between GAG content and either 10% instantaneous modulus ($p < 0.0001$, $R^2 = 0.746$) or 10% relaxation modulus ($p < 0.0001$, $R^2 = 0.723$). The 10% coefficient of viscosity also exhibited a relatively strong correlation to GAG content ($p < 0.0001$, $R^2 = 0.570$). Similar correlations were observed between GAG content and compressive properties measured at 20% strain.

Correlations displayed moderated strength between collagen or pyridinoline content and construct tensile properties. When examined separately, circumferential Young's modulus increased with collagen/DW ($p < 0.0001$, $R^2 = 0.445$) and circumferential UTS increased with pyridinoline/DW ($p < 0.0001$, $R^2 = 0.451$) (Fig. 6). Statistically significant, but weaker, correlations were observed between collagen and circumferential UTS, pyridinoline and circumferential Young's modulus, and collagen or pyridinoline with radial tensile properties. When both collagen and pyridinoline were included in the statistical models, correlations with tensile properties became stronger ($R^2_{adj} > 0.5$; Fig. 6B and C). In the two-factor models, collagen cross-links correlated with tensile properties, contributing 67% of the tensile strength of engineered tissues. Additionally, collagen was estimated to contribute 62% of circumferential tensile stiffness and 33% of circumferential UTS. Importantly, collagen and pyridinoline were weakly correlated with each other ($p = 0.0004$; $R^2 = 0.170$). The scaled prediction expressions for circumferential tensile properties are given by the equations that follow.

$$UTS_{circ} = 0.596(MPa) + 0.138(MPa)\cdot\frac{Col - 0.0960}{0.0524}(g/gDW) + 0.286(MPa\cdot g/nmol)\cdot\frac{Pyr - 348}{523}(nmol/gDW)$$

$$E_{Y,circ} = 2.44(MPa) + 1.26(MPa)\cdot\frac{Col - 0.0960}{0.0524}(g/gDW) + 0.76(MPa\cdot g/nmol)\cdot\frac{Pyr - 348}{523}(nmol/gDW)$$

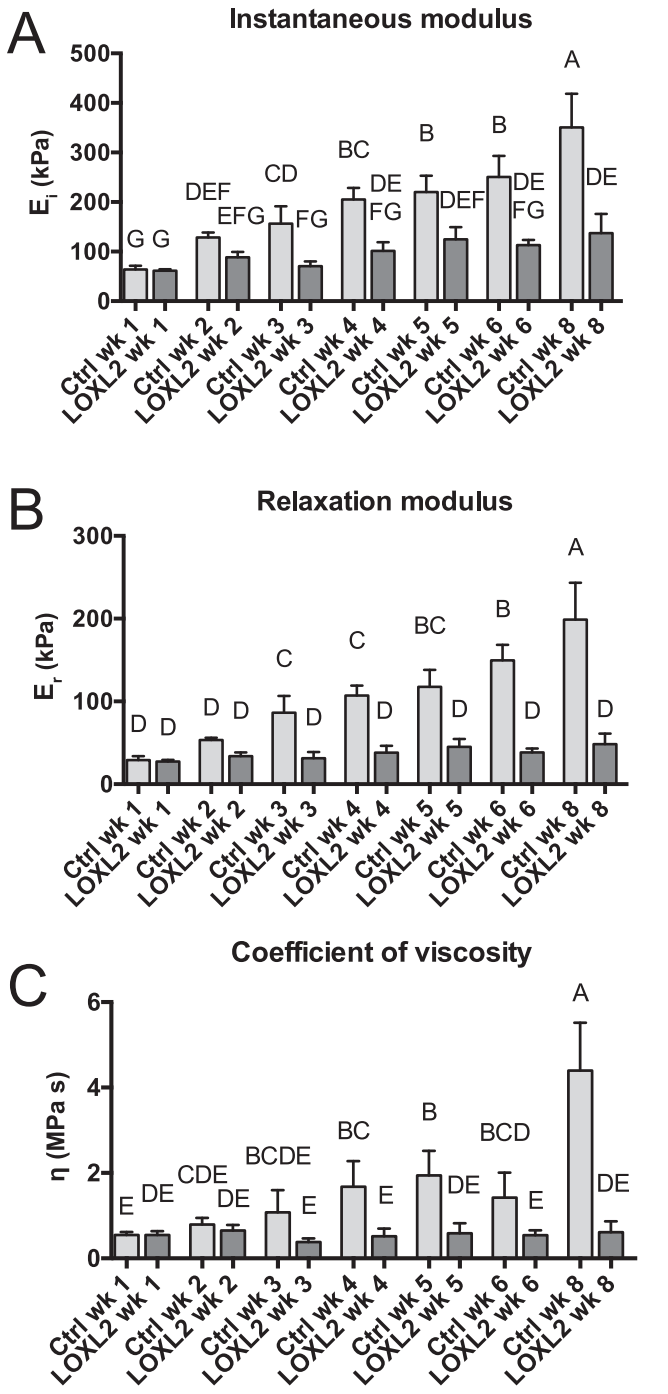

Fig. 4. Compressive properties of self-assembling, meniscus-shaped fibrocartilage. Native tissue values: 465 ± 110 kPa (instantaneous modulus), 51 ± 20 kPa (relaxation modulus), 2.78 ± 1.29 MPa·s (coefficient of viscosity). Groups lacking a letter in common are significantly different.

3.6. qMRI

Representative MR images of samples from each group are displayed in Fig. 7A. One-way ANOVA confirmed a significant effect of treatment group on T1 time ($p = 0.028$), but no differences among groups were determined to be significant by Tukey's *post hoc* test. To determine if LOXL2 treatment had any effect on construct T1 time, the difference between control and LOXL2-treated constructs was assessed by *post hoc* least square means contrast; the T1 time of LOXL2-treated constructs was found to be significantly lower than that of control constructs ($p = 0.028$) (Fig. 7B). T2 times of control constructs increased from 2 weeks (20.8 ± 2.8 ms) to 8 weeks (45.0 ± 2.9 ms) in culture (Fig. 7B). At 8 weeks, the T2 times of control constructs were greater than those of all LOXL2-treated constructs. T2 times varied minimally among LOXL2-treated constructs at different culture durations from 33.2 ± 7.3 ms at 2 weeks to 28.5 ± 4.9 ms at 8 weeks, and no significant differences were observed. ADC tended to decrease with increasing culture duration regardless of LOXL2 treatment from $1.84 \pm 0.20 \times 10^{-3}$ mm^2/s at two weeks of culture to $1.66 \pm 0.10 \times 10^{-3}$ mm^2/s at 8 weeks of culture, but there were no significant differences among treatment groups or culture durations.

Several statistically significant correlations were observed among qMRI metrics and biochemical composition or mechanical properties of the fibrocartilage constructs (Fig. 7C and D). Construct T2 times moderately correlated with GAG/DW ($p < 0.0001$; $R^2 = 0.338$) and with pyridinoline/DW ($p = 0.0001$; $R^2 = 0.338$). There was no significant correlation between GAG/DW and pyridinoline/DW ($p = 0.06$, $R^2 = 0.052$). T1 time weakly correlated with pyridinoline/DW ($p = 0.0005$; $R^2 = 0.214$). T2 time also correlated with the compressive properties of fibrocartilage constructs. Specifically, T2 time moderately correlated with 10% relaxation modulus ($p < 0.0001$; $R^2 = 0.379$), 10% instantaneous modulus ($p < 0.0001$; $R^2 = 0.342$), and 10% coefficient of viscosity ($p < 0.0001$; $R^2 = 0.389$). Significant, but slightly weaker correlations were observed between T2 time and the 20% compressive properties. Weak, inverse correlations were observed between T2 time and tensile properties, including circumferential UTS ($p = 0.0026$; $R^2 = 0.210$), radial UTS ($p = 0.028$; $R^2 = 0.130$), and radial Young's modulus ($p = 0.024$; $R^2 = 0.137$). No multi-factor models were identified by stepwise regression for which all factors made statistically significant contributions to qMRI properties.

3.7. Scanning electron microscopy

Longer duration culture, especially in the LOXL2-treated constructs, resulted in increases in ECM density and average fiber diameter (Fig. 8). ECM density increased in all groups over time, with control and LOXL2-treated constructs cultured for 8 weeks displaying the highest overall densities. Increased fiber diameters were observable beginning at week 4 for the LOXL2-treated constructs and week 6 for the control constructs. The thickest collagen fibers were found in the LOXL2-treated constructs, with average fiber diameters reaching 87 ± 19 nm and 88 ± 16 nm for the week 6 and week 8 time points, respectively. At week 8, the LOXL2-treated constructs displayed a 25% increase in average fiber diameter compared to control constructs' average fiber diameter of 71 ± 13 nm.

4. Discussion

This study examined the temporal development of pyridinoline cross-links, and their contribution to the mechanical properties and quantitative imaging characteristics of tissue engineered fibrocartilage. Experimental results supported the following hypotheses that motivated this study: (i) pyridinoline cross-links increased over time in all fibrocartilage constructs and increased more in constructs treated with LOXL2; (ii) pyridinoline cross-link content was a significant contributor to the tensile properties of self-assembling fibrocartilage alongside collagen content; and (iii) biochemical composition and mechanical properties of self-assembling fibrocartilage correlated with one or more qMRI metrics. This is the first study to demonstrate near-native cross-link content in an engineered tissue, and the first study to quantify

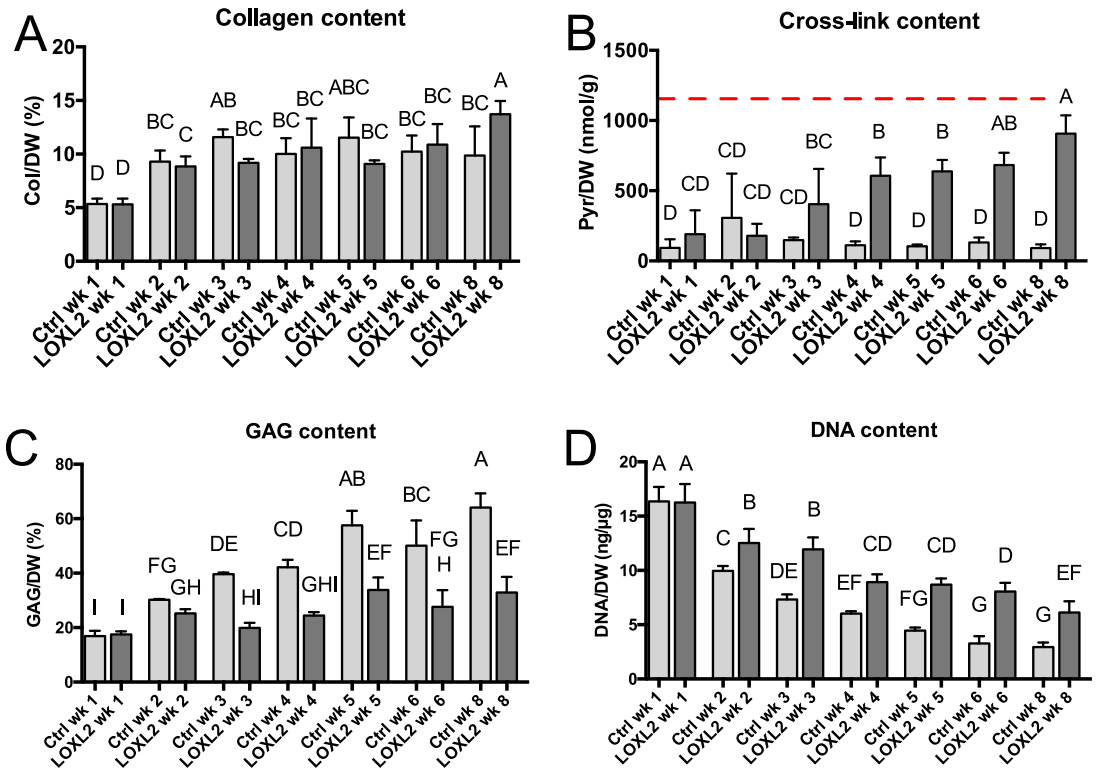

Fig. 5. Biochemical content of self-assembling, meniscus-shaped fibrocartilage. Dashed line in second panel indicates cross-link content of native tissue. Native tissue values: 72.0 ± 3.2% (collagen/DW), 1180 ± 242 nmol/g (Pyr/DW), 1.7 ± 0.4% (GAG/DW), 0.55 ± 0.06 ng/μg (DNA/DW). Groups lacking a letter in common are significantly different.

pyridinoline cross-link development over time in a self-assembling tissue. Additionally, this work shows the relative contributions of collagen and pyridinoline to the tensile properties of collagenous tissue for the first time. Furthermore, this is the first investigation to identify a relationship between qMRI metrics and the pyridinoline cross-link content of an engineered collagenous tissue.

Collagen and pyridinoline cross-link content both significantly contributed to the tensile properties of self-assembling fibrocartilage in this study. The results indicate that the properties of engineered cartilage treated with LOXL2 are comparable with, or superior to, those of untreated control tissues. This corroborates past studies applying exogenous LOXL2 in engineered tissues [13,34]. This investigation demonstrated, for the first time, engineered cartilage with cross-link content at 77% of native tissue values. To the best of our knowledge, prior work with engineered tissue has achieved cross-link content of no more than 25–45% of native tissue values [13,15]. In addition to the increases in cross-link content, tensile properties vastly increased with LOXL2 treatment, reaching up to 3.7-fold of control values. This result confirms previous work suggesting that pyridinoline contributes to the tensile properties of collagen networks in native tissues [35–37]. Furthermore, the results of the current study quantify the relative contributions of both collagen and pyridinoline cross-links to tensile stiffness and strength. In a two-factor model of tensile properties, the collagen content of self-assembling fibrocartilage was responsible for 62% of its tensile stiffness and pyridinoline cross-links were responsible for 67% of its tensile strength. Knowing the relative contributions of collagen and pyridinoline to tensile properties, and defining other factors that contribute to tensile properties, will help inform tissue engineering efforts toward replicating the tensile stiffness and strength of native musculoskeletal tissues.

The compressive properties and GAG content measured in this study reflect the need for additional work exploring the modulation of these properties in engineered cartilage. Overall, the compressive properties for LOXL2-treated constructs in this study were similar to native tissue values. Specifically, the relaxation modulus for LOXL2-treated constructs closely matched native tissue values while the instantaneous modulus was greater in the control constructs. Similarly, GAG content in control constructs exceeded native tissue values, while LOXL2-treated constructs were more like native tissue values in terms of GAG content. This agrees with previous results in cartilage tissue engineering, demonstrating overproduction of GAG as compared to native tissue [38]. It is possible that signaling effects of LOXL2 may depress GAG production, as members of the LOX family of proteins have been shown to bind and sequester endogenous TGF-β1 activity in bone [39]. Promotion of GAG synthesis via TGF-β1 and preventing excess GAG production using chondroitinase-ABC may bring engineered construct compressive properties closer to native tissue compressive properties [8,40].

The qMRI metrics of T1 and T2 times correlated with important functional properties of self-assembling fibrocartilage in this study. Considerable research has examined the relationship between various qMRI parameters and functional properties of native hyaline articular cartilage [22,23] as well as tissue engineered cartilage [41]. Although several qMRI metrics are described in the literature, T1 and T2 times were chosen because these measurements can be performed without specialized hardware, pulse sequences, or exogenous contrast media. T1 and T2 times characterize the recovery of longitudinal magnetization and the decay of transverse magnetization, respectively, following excitation of protons in the magnetic field of an MRI system. T1 and T2 times are likely influenced by more than a single biochemical component of the cartilage extracellular matrix; however, T2 time is known to be influenced by collagen content and fiber orientation [22,23]. The current study found a significant correlation between the T2 time and the GAG content of fibrocartilage constructs similar to

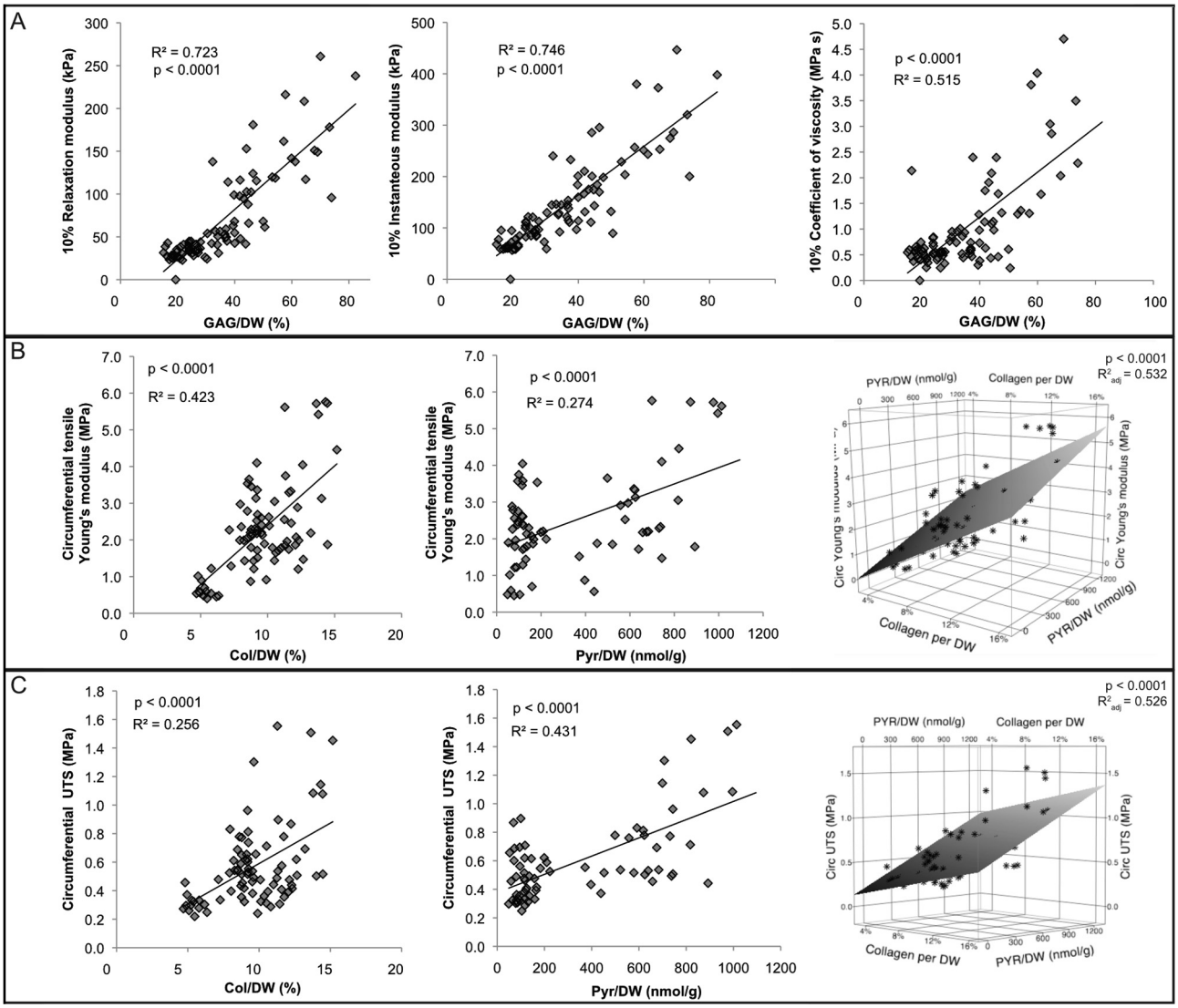

Fig. 6. Correlations among collagen, pyridinoline, and tensile properties.

previously reported findings [25]. It is likely that in the absence of collagen fiber alignment, T2 time becomes sensitive to changes in the content of other macromolecules, such as GAG. Importantly, this study found significant, inverse correlations between pyridinoline cross-links and both T1 time and T2 time of self-assembling fibrocartilage. These findings corroborate recent work demonstrating a relationship between qMRI metrics and cross-link content in native articular cartilage [42]. It is known that molecular size and rate of molecular motion in a tissue influences the tissue's T1 and T2 times [43]. Pyridinoline cross-links likely increase the effective molecular size and decrease the rate of molecular motion throughout the collagen network, possibly explaining the observed decreases of T1 and T2 times in fibrocartilage constructs with a relatively large concentration of pyridinoline cross-links. Although our results did not identify a single best model that clearly relates multiple biochemical properties to the T1 and T2 times of self-assembled fibrocartilage constructs, both GAG and pyridinoline content seem to influence the constructs' T2 times. One potential limitation of this investigation is that not every construct was assessed with qMRI. Future research examining a larger number of constructs may elucidate contributions from multiple macromolecules to the qMRI properties of self-assembled fibrocartilage.qMRI parameters have been correlated with native cartilage and tissue engineered cartilage compressive properties [23]. The T2 time of fibrocartilage constructs in this study was significantly correlated with their compressive stiffness and coefficient of viscosity. A previous study found a similar correlation between T2 time and equilibrium compressive modulus [25]. This finding is most likely due to strong correlations between GAG content and construct compressive properties. T2 time also weakly, inversely correlated with the tensile properties of fibrocartilage constructs. In this study, no significant differences were observed in the ADC of self-assembled fibrocartilage constructs associated with culture duration or LOXL2 treatment. Previous studies reported mixed results regarding ADC and correlations with properties of tissue-engineered and native cartilage [25,44–46]. The direction of diffusion in native cartilage samples is highly anisotropic and associated with collagen alignment [47,48], and it is possible that measuring diffusion in multiple directions by diffusion tensor imaging is necessary to further assess potential changes in diffusion in developing self-assembled fibrocartilage constructs. Indeed, one possible limitation of this investigation is that only slices of constructs, rather than their full volumes, were examined with qMRI. The correlations between qMRI parameters and functional properties demonstrate that qMRI can be used to non-destructively assess important qualities, including GAG content,

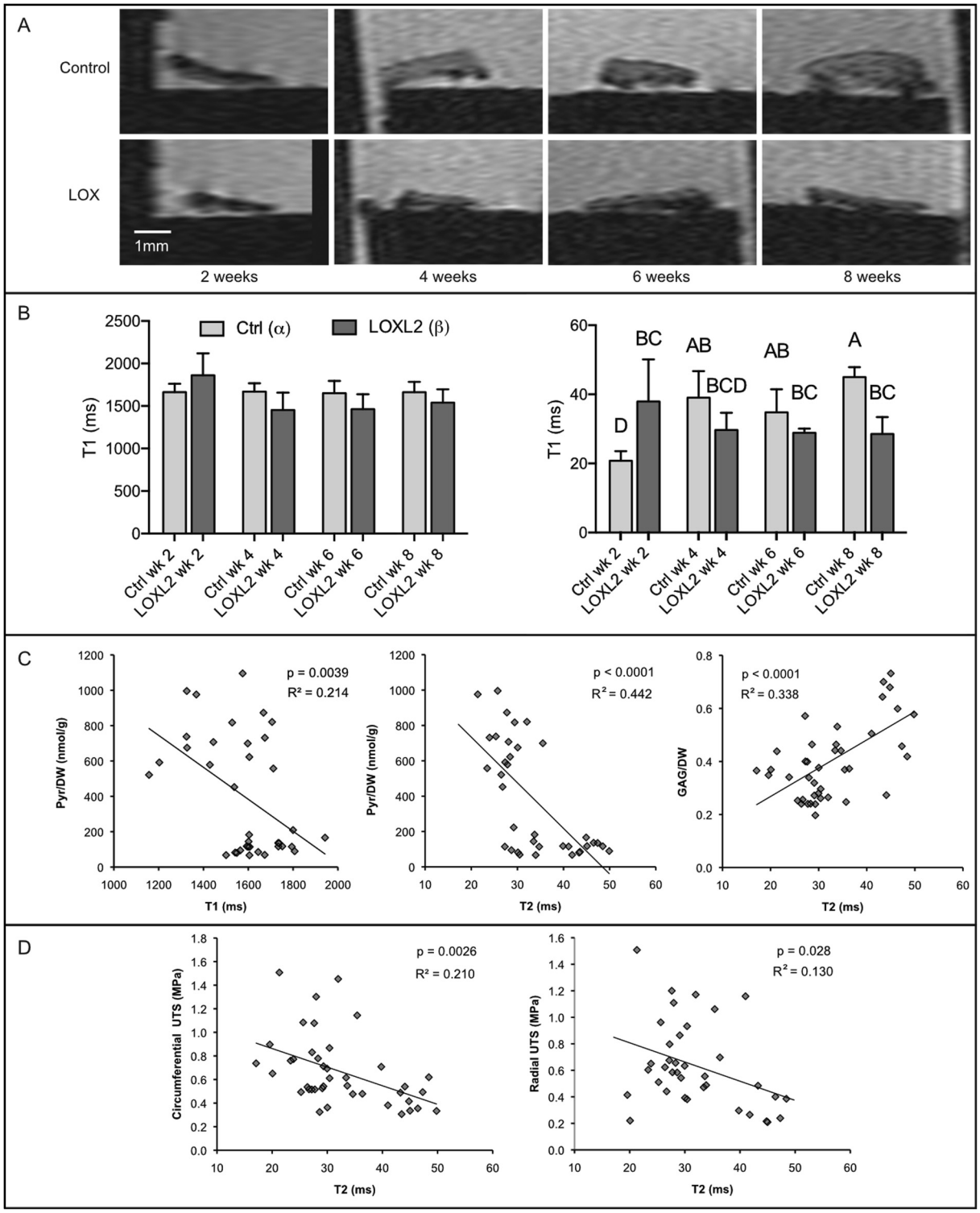

Fig. 7. MRI appearance, quantitative MRI results, and correlations with functional properties. Groups lacking a letter in common are significantly different.

pyridinoline cross-link formation, and mechanical properties, of tissue engineered fibrocartilage.

The temporal characterization of LOXL2 and its effects performed in this investigation paves the way for further research in increasing mechanical properties of engineered tissues. This research found that pyridinoline cross-links significantly increased within three weeks of initiating LOXL2 treatment. Beginning at week 4 specifically, cross-link content for LOXL2 treated constructs increased significantly over control constructs, reaching 606.74 ± 130.22 nmol/g as compared to 111.68 ± 27.76 nmol/g. Other biophysical and/or biochemical stimuli, such as chondroitinase-ABC, may act additively or synergistically when their application is timed carefully and combined with LOXL2. Previous work has shown that chondroitinase-ABC increases tensile properties of engineered tissues with and without LOXL2, but comparing different time points in combination with LOXL2 treatment remains unexplored [49]. Another benefit of elucidating the temporal development of pyridinoline cross-links pertains to

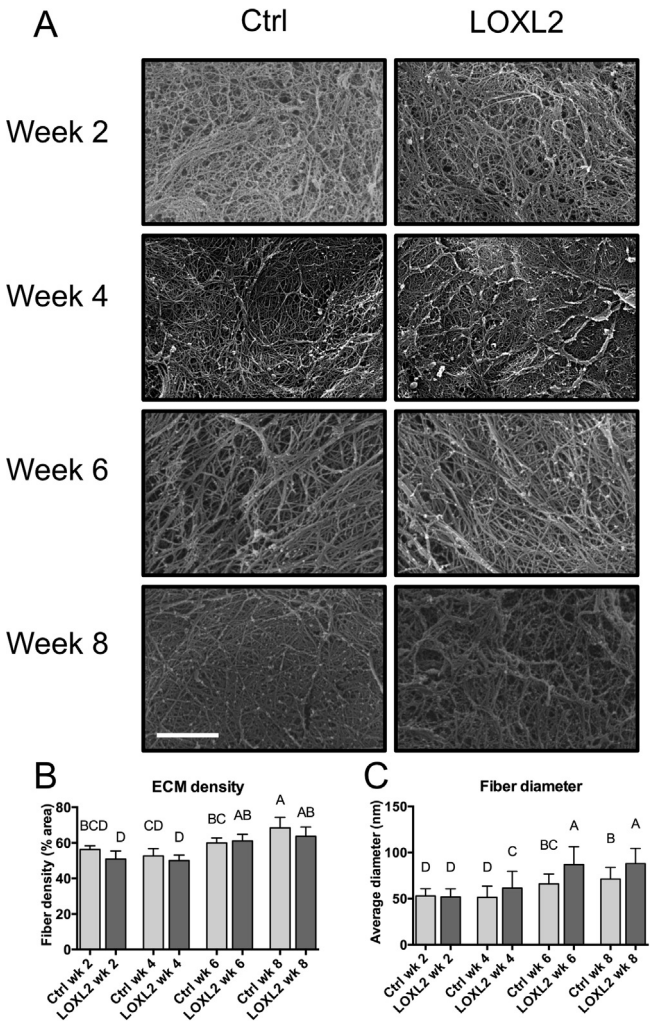

Fig. 8. Scanning electron micrographs of the collagen matrix of self-assembling, meniscus-shaped fibrocartilage. Scale bar in lower left represents 2 μm. Groups lacking a letter in common are significantly different.

integration of engineered tissue with native tissue. One potential limitation of this study was that continuous LOX treatment was not administered. Prior work reported no difference between single and multiple LOXL2 treatment in terms of mechanical integration [49]; this is likely because precise timing, coinciding with pyridinoline cross-link formation, was not employed. Waiting a minimum of three weeks from the initiation of LOXL2 treatment, or treating engineered tissues continuously with LOX, may be necessary to observe beneficial effects towards tissue integration.

Treating self-assembling fibrocartilage with LOXL2 has the potential to improve or preserve construct properties during long-term culture. The results of this study found that LOXL2-treated constructs maintained their compressive properties and demonstrated increasing tensile properties throughout 8 weeks of culture. At week 8, LOXL2 treated constructs displayed circumferential stiffness and strength of 5.65 ± 0.14 MPa and 1.34 ± 0.22 MPa, respectively, which represented an increase over all other LOXL2 treated constructs at various time points. By contrast, although control constructs exhibited greater compressive properties associated with excessive GAG concentrations, the tensile properties of control constructs tended to decline in the last 3 to 4 weeks of culture. For example, circumferential Young's modulus in control constructs declined from 2.98 ± 0.64 MPa in week 6 to 1.77 ± 0.49 MPa in week 8. A similar decline was observed in the radial Young's modulus of control constructs, which decreased from 2.12 ± 0.87 MPa in week 6 to 0.94 ± 0.29 MPa in week 8. Indeed, one possible limitation of this study was that it stopped after week 8 of culture, and did not proceed with investigation of even longer duration cultures. Maintenance of tissue properties via LOXL2 administration during long culture durations will allow for examination of engineered constructs over multiple consecutive months of tissue growth.

This study investigated LOXL2 treatment on self-assembling knee menisci, and the resulting mechanical, biochemical, and quantitative imaging properties of the growing tissue over time. Engineered tissues treated with LOXL2 displayed near-native cross-link content, with values reaching 77% of native values. Pyridinoline content was found to be a significant driver of tensile integrity, especially tensile strength. Lastly, measured qMRI parameters, and in particular T2, were found to correlate with cross-link content, GAG content, and mechanical properties. These results emphasize the potential for MRI methodologies to non-destructively assess engineered constructs, and the importance of pyridinoline cross-links in collagen-rich tissues. Because of the important role of pyridinoline in growing fibrocartilage, it is imperative that additional work is performed quantifying cross-link content over time in other collagen-rich engineered tissues such as articular cartilage, tendon, bone, skin, and vasculature.

Role of the funding source

This investigation was funded by NIH grant R01 AR067821. DDC was funded in part by an NIH T32 fellowship (OD011147). The funding sources had no role in study design, data collection, data analysis or interpretation, or preparation and submission of this work for publication.

References

[1] G.D. Abrams, R.M. Frank, A.K. Gupta, J.D. Harris, F.M. McCormick, B.J. Cole, Trends in meniscus repair and meniscectomy in the United States, 2005–2011, Am. J. Sports Med. 41 (2013) 1–16, https://doi.org/10.1177/0363546513495641.
[2] M.A. Sweigart, K.A. Athanasiou, Toward tissue engineering of the knee meniscus, Tissue Eng. 7 (2001) 111–129, https://doi.org/10.1089/107632701300062697.
[3] E.A. Makris, P. Hadidi, K.A. Athanasiou, The knee meniscus: structure-function, pathophysiology, current repair techniques, and prospects for regeneration, Biomaterials 32 (2011) 1–21, https://doi.org/10.1016/j.biomaterials.2011.06.037.
[4] M.J. Salata, A.E. Gibbs, J.K. Sekiya, A systematic review of clinical outcomes in patients undergoing meniscectomy, Am. J. Sports Med. 38 (2010) 1907–1916, https://doi.org/10.1177/0363546510370196.
[5] R. Verdonk, H. Madry, N. Shabshin, F. Dirisamer, G.M. Peretti, N. Pujol, T. Spalding, P. Verdonk, R. Seil, V. Condello, B. Di Matteo, J. Zellner, P. Angele, The role of meniscal tissue in joint protection in early osteoarthritis, Knee Surg. Sports Traumatol. Arthrosc. 24 (2016) 1763–1774, https://doi.org/10.1007/s00167-016-4069-2.
[6] J.C. Hu, K.A. Athanasiou, A self-assembling process in articular cartilage tissue engineering, Tissue Eng. 12 (2006) 969–979, https://doi.org/10.1089/ten.2006.12.969.
[7] G.M. Hoben, J.C. Hu, R.A. James, K.A. Athanasiou, Self-assembly of fibrochondrocytes and chondrocytes for tissue engineering of the knee meniscus, Tissue Eng. 13 (2007) 939–946, https://doi.org/10.1089/ten.2006.0116.
[8] D.J. Huey, K.A. Athanasiou, Maturational growth of self-assembled, functional menisci as a result of TGF-β1 and enzymatic chondroitinase-ABC stimulation, Biomaterials 32 (2011) 2052–2058, https://doi.org/10.1016/j.biomaterials.2010.11.041.
[9] K.A. Athanasiou, R. Eswaramoorthy, P. Hadidi, J.C. Hu, Self-organization and the self-assembling process in tissue engineering, Annu. Rev. Biomed. Eng. 15 (2013) 115–136, https://doi.org/10.1146/annurev-bioeng-071812-152423.
[10] K.N. Hauch, D.F. Villegas, T.L. Haut Donahue, Geometry, time-dependent and failure properties of human meniscal attachments, J. Biomech. 43 (2010) 463–468, https://doi.org/10.1016/j.jbiomech.2009.09.043.
[11] P.G. Bullough, L. Munuera, J. Murphy, A.M. Weinstein, The strength of the menisci of the knee as it relates to their fine structure, J. Bone Joint Surg. 52 (1970) 564–567.

[12] G.M. Williams, R.L. Sah, In vitro modulation of cartilage shape plasticity by biochemical regulation of matrix remodeling, Tissue Eng. A 17 (2011) 17–23, https://doi.org/10.1089/ten.TEA.2010.0177.
[13] E.A. Makris, D.J. Responte, N.K. Paschos, J.C. Hu, K.A. Athanasiou, Developing functional musculoskeletal tissues through hypoxia and lysyl oxidase-induced collagen cross-linking, Proc. Natl. Acad. Sci. U.S.A. 111 (2014) E4832–E4841, https://doi.org/10.1073/pnas.1414271111.
[14] Y.M. Bastiaansen-Jenniskens, W. Koevoet, A.C.W. de Bart, J.C. van der Linden, A. M. Zuurmond, H. Weinans, J.A.N. Verhaar, G.J.V.M. van Osch, J. DeGroot, Contribution of collagen network features to functional properties of engineered cartilage, Osteoarthritis Cartil. 16 (2008) 359–366, https://doi.org/10.1016/j.joca.2007.07.003.
[15] E.A. Makris, R.F. MacBarb, D.J. Responte, J.C. Hu, K.A. Athanasiou, A copper sulfate and hydroxylysine treatment regimen for enhancing collagen cross-linking and biomechanical properties in engineered neocartilage, FASEB J. 27 (2013) 2421–2430, https://doi.org/10.1096/fj.12-224030.
[16] D.R. Eyre, J.-J. Wu, Collagen cross-links, Top. Curr. Chem. 247 (2005) 207–229, https://doi.org/10.1007/b103828.
[17] D.R. Eyre, M.A. Weis, J.J. Wu, Maturation of collagen ketoimine cross-links by an alternative mechanism to pyridinoline formation in cartilage, J. Biol. Chem. 285 (2010) 16675–16682, https://doi.org/10.1074/jbc.M110.111534.
[18] D.R. Eyre, M.A. Weis, J.-J. Wu, Advances in collagen cross-link analysis, Methods 45 (2008) 65–74, https://doi.org/10.1016/j.ymeth.2008.01.002.
[19] W.M. Elbjeirami, E.O. Yonter, B.C. Starcher, J.L. West, Enhancing mechanical properties of tissue-engineered constructs via lysyl oxidase crosslinking activity, J. Biomed. Mater. Res. 66 (2003) 513–521, https://doi.org/10.1002/jbm.a.10021.
[20] K.M. Reiser, J.A. Last, Biosynthesis of collagen crosslinks: vivo labelling of neonatal skin, tendon, and bone in rats, Connect Tissue Res. 14 (2009) 293–306, https://doi.org/10.3109/03008208609017472.
[21] T. Ahsan, F. Harwood, K.B. McGowan, D. Amiel, R.L. Sah, Kinetics of collagen crosslinking in adult bovine articular cartilage, Osteoarthritis Cartil. 13 (2005) 709–715, https://doi.org/10.1016/j.joca.2005.03.005.
[22] D.A. Binks, R.J. Hodgson, M.E. Ries, R.J. Foster, S.W. Smye, D. McGonagle, A. Radjenovic, Quantitative parametric MRI of articular cartilage: a review of progress and open challenges, Br. J. Radiol. 86 (2014) 20120163, https://doi.org/10.1259/bjr.20120163.
[23] D.D. Chan, C.P. Neu, Probing articular cartilage damage and disease by quantitative magnetic resonance imaging 20120608 20120608, J.R. Soc. Interface 10 (2013), https://doi.org/10.1098/rsif.2012.0608.
[24] S. Miyata, K. Homma, T. Numano, T. Tateishi, T. Ushida, Evaluation of negative fixed-charge density in tissue-engineered cartilage by quantitative MRI and relationship with biomechanical properties, J. Biomech. Eng. 132 (2010) 071014, https://doi.org/10.1115/1.4001369.
[25] S. Miyata, T. Numano, K. Homma, T. Tateishi, T. Ushida, Feasibility of noninvasive evaluation of biophysical properties of tissue-engineered cartilage by using quantitative MRI, J. Biomech. 40 (2007) 2990–2998, https://doi.org/10.1016/j.jbiomech.2007.02.002.
[26] J.E. Novotny, C.M. Turka, C. Jeong, A.J. Wheaton, C. Li, A. Presedo, D.W. Richardson, R. Reddy, G.R. Dodge, Biomechanical and magnetic resonance characteristics of a cartilage-like equivalent generated in a suspension culture, Tissue Eng. 12 (2006) 2755–2764, https://doi.org/10.1089/ten.2006.12.2755.
[27] H. Xu, S.F. Othman, R.L. Magin, Monitoring tissue engineering using magnetic resonance imaging, J. Biosci. Bioeng. 106 (2008) 515–527.
[28] J. Sanchez-Adams, K.A. Athanasiou, Regional effects of enzymatic digestion on knee meniscus cell yield and phenotype for tissue engineering, Tissue Eng. C Meth. 18 (2012) 235–243, https://doi.org/10.1089/ten.TEC.2011.0383.
[29] P. Hadidi, K.A. Athanasiou, Enhancing the mechanical properties of engineered tissue through matrix remodeling via the signaling phospholipid lysophosphatidic acid, Biochem. Biophys. Res. Commun. 433 (2013) 133–138, https://doi.org/10.1016/j.bbrc.2013.02.048.
[30] P. Hadidi, T.C. Yeh, J.C. Hu, K.A. Athanasiou, Critical seeding density improves the properties and translatability of self-assembling anatomically shaped knee menisci, Acta Biomater. 11 (2014) 1–10, https://doi.org/10.1016/j.actbio.2014.09.011.
[31] K.D. Allen, K.A. Athanasiou, Viscoelastic characterization of the porcine temporomandibular joint disc under unconfined compression, J. Biomech. 39 (2006) 312–322, https://doi.org/10.1016/j.jbiomech.2004.11.012.
[32] G.K. Reddy, C.S. Enwemeka, A simplified method for the analysis of hydroxyproline in biological tissues, Clin. Biochem. 29 (1996) 225–229.
[33] R.A. Bank, B. Beekman, N. Verzijl, J.A. de Roos, A.N. Sakkee, J.M. TeKoppele, Sensitive fluorimetric quantitation of pyridinium and pentosidine crosslinks in biological samples in a single high-performance liquid chromatographic run, J. Chromatogr. B Biomed. Sci. Appl. 703 (1997) 37–44.
[34] A.A. Athens, E.A. Makris, J.C. Hu, Induced collagen cross-links enhance cartilage integration, PLoS One 8 (2013) e60719–6, https://doi.org/10.1371/journal.pone.0060719.
[35] C. Frank, D. McDonald, J. Wilson, D. Eyre, N. Shrive, Rabbit medial collateral ligament scar weakness is associated with decreased collagen pyridinoline crosslink density, J. Orthop. Res. 13 (1995) 157–165, https://doi.org/10.1002/jor.1100130203.
[36] A.K. Williamson, A.C. Chen, K. Masuda, E.J.M.A. Thonar, R.L. Sah, Tensile mechanical properties of bovine articular cartilage: variations with growth and relationships to collagen network components, J. Orthop. Res. 21 (2003) 872–880, https://doi.org/10.1016/S0736-0266(03)00030-5.
[37] J.E. Marturano, J.F. Xylas, G.V. Sridharan, I. Georgakoudi, C.K. Kuo, Lysyl oxidase-mediated collagen crosslinks may be assessed as markers of functional properties of tendon tissue formation, Acta Biomater. 10 (2014) 1370–1379, https://doi.org/10.1016/j.actbio.2013.11.024.
[38] R.M. Natoli, D.J. Responte, B.Y. Lu, K.A. Athanasiou, Effects of multiple chondroitinase ABC applications on tissue engineered articular cartilage, J. Orthop. Res. 27 (2009) 949–956, https://doi.org/10.1002/jor.20821.
[39] P. Atsawasuwan, Y. Mochida, M. Katafuchi, M. Kaku, K.S.K. Fong, K. Csiszar, M. Yamauchi, Lysyl oxidase binds transforming growth factor-beta and regulates its signaling via amine oxidase activity, J. Biol. Chem. 283 (2008) 34229–34240, https://doi.org/10.1074/jbc.M803142200.
[40] L. Bian, K.M. Crivello, K.W. Ng, D. Xu, D.Y. Williams, G.A. Ateshian, C.T. Hung, Influence of temporary chondroitinase ABC-induced glycosaminoglycan suppression on maturation of tissue-engineered cartilage, Tissue Eng. A 15 (2009) 2065–2072, https://doi.org/10.1089/ten.tea.2008.0495.
[41] M. Kotecha, D. Klatt, R.L. Magin, Monitoring cartilage tissue engineering using magnetic resonance spectroscopy, imaging, and elastography, Tissue Eng. B Rev. 19 (2013) 470–484, https://doi.org/10.1089/ten.TEB.2012.0755.
[42] J. Rautiainen, M.T. Nieminen, E.-N. Salo, H.T. Kokkonen, S. Mangia, S. Michaeli, O. Gröhn, J.S. Jurvelin, J. Töyräs, M.J. Nissi, Effect of collagen cross-linking on quantitative MRI parameters of articular cartilage, Osteoarthritis Cartil. /OARS, Osteoarthritis Res. Soc. 24 (2016) 1656–1664, https://doi.org/10.1016/j.joca.2016.04.017.
[43] J.T. Bushberg, J.A. Seibert, E.M. Leidholdt, J.M. Boone, E.J. Goldschmidt, The essential physics of medical imaging 1936 1936, Med. Phys. 30 (2003), https://doi.org/10.1118/1.1585033.
[44] S. Ravindran, M. Kotecha, C.-C. Huang, A. Ye, P. Pothirajan, Z. Yin, R. Magin, A. George, Biological and MRI characterization of biomimetic ECM scaffolds for cartilage tissue regeneration, Biomaterials 71 (2015) 58–70, https://doi.org/10.1016/j.biomaterials.2015.08.030.
[45] V. Juras, M. Bittsansky, Z. Majdisova, P. Szomolanyi, I. Sulzbacher, S. Gäbler, J. Stampfl, G. Schüller, S. Trattnig, In vitro determination of biomechanical properties of human articular cartilage in osteoarthritis using multi-parametric MRI, J. Magn. Reson. 197 (2009) 40–47, https://doi.org/10.1016/j.jmr.2008.11.019.
[46] T. Aoki, A. Watanabe, N. Nitta, T. Numano, M. Fukushi, M. Niitsu, Correlation between apparent diffusion coefficient and viscoelasticity of articular cartilage in a porcine model, Skeletal Radiol. 41 (2012) 1087–1092, https://doi.org/10.1007/s00256-011-1340-y.
[47] T. Azuma, R. Nakai, O. Takizawa, S. Tsutsumi, In vivo structural analysis of articular cartilage using diffusion tensor magnetic resonance imaging, Magn. Reson. Imag. 27 (2009) 1242–1248, https://doi.org/10.1016/j.mri.2009.05.012.
[48] S.K. de Visser, J.C. Bowden, E. Wentrup-Byrne, L. Rintoul, T. Bostrom, J.M. Pope, K.I. Momot, Anisotropy of collagen fibre alignment in bovine cartilage: comparison of polarised light microscopy and spatially resolved diffusion-tensor measurements, Osteoarthritis Cartil. 16 (2008) 689–697, https://doi.org/10.1016/j.joca.2007.09.015.
[49] E.A. Makris, R.F. MacBarb, N.K. Paschos, J.C. Hu, K.A. Athanasiou, Combined use of chondroitinase-ABC, TGF-β1, and collagen crosslinking agent lysyl oxidase to engineer functional neotissues for fibrocartilage repair, Biomaterials 35 (2014) 6787–6796, https://doi.org/10.1016/j.biomaterials.2014.04.083.